Mechanism of Electrocatalytic Reduction of Nitric Oxide on Pt(100)

Victor Rosca* and Marc T. M. Koper

Schuit Institute of Catalysis, Laboratory of Inorganic Chemistry and Catalysis, Eindhoven University of Technology, 5600 MB Eindhoven, The Netherlands

Received: June 3, 2005; In Final Form: July 14, 2005

The mechanism of electrocatalytic reduction of nitric oxide on Pt(100)-(1 × 1) in acidic media has been studied using voltammetry, in-situ infrared spectroscopy, and on-line mass spectroscopy, considering the effect of surface defects, NO coverage, and the nature of the supporting electrolyte (sulfate vs perchlorate). Related mechanistic aspects of hydroxylamine (HAM) transformations on the same surface have been also examined. The adsorption of nitric oxide on Pt(100) results in the formation of an adlayer with a structure similar to that formed under ultrahigh vacuum (UHV) conditions. Ammonia was shown to be the main product of NO_{ads} reduction on Pt(100). The saturation coverage of NO adsorbate on Pt(100) was found to be around 0.5 ML, in agreement with previous UHV and electrochemical studies. Two features observed in the voltammetric profile for the electrocatalytic reduction of saturated and subsaturated NO adlayers were tentatively ascribed to reactions of NO species having different reactivity. The Tafel slope analysis of these voltammetric features gives values of ca. 60 mV decade^{-1}. This value was interpreted in terms of an EC mechanism, in which the first electron/proton transfer is at equilibrium, resulted in formation of HNO_{ads} intermediate, while the second reaction step is a chemical rate-determining step. This chemical step is assumed to involve the N−O bond breaking in HNO_{ads} intermediate, which most probably requires a free neighboring site. From a comparison with NO_{ads} reduction on Pt(111) and Pt(110), it follows that (i) the reaction mechanism is structure sensitive and (ii) Pt(100) is the most active surface for breaking the N−O bond, which is in agreement with the trend observed under UHV conditions. As suggested in our previous studies, the electrocatalytic reduction of HAM is likely to proceed through its partial dehydrogenation. In this study, we further develop this idea, and, based on the mechanism for NO_{ads} reduction proposed here, we suggest HNO_{ads} to be the intermediate appearing both in HAM reduction/oxidation and in NO_{ads} reduction.

1. Introduction

Adsorption and reactions of nitric oxide on transition metal surfaces in an electrochemical environment are of considerable practical importance, mainly in connection with the industrial synthesis of hydroxylamine as well as with environmentally important removal of nitrate, nitrite, and nitric oxide itself. Nitric oxide adsorbs strongly on transition metals and is a key intermediate in many electrochemical transformations of inorganic nitrogen-containing compounds.[1] From a fundamental point of view, reactions of NO on single-crystal transition metal surfaces, particularly NO reduction, are attractive for carrying out model studies in heterogeneous electrocatalysis as well as for comparing reactions at the metal−gas and metal−liquid interfaces.

Adsorption and electrochemical transformations of NO on single-crystal platinum surfaces, as well as on other transition metal surfaces, have been intensively studied in recent years.[2−18] These studies resulted in a significant insight into the structure and reactivity of NO adlayers, as compared to earlier studies on polycrystalline platinum.[19]

In a recent detailed voltammetric study on Pt(111), Pt(110), and a series of stepped Pt[*n*(111) × (111)] electrodes, we have shown that the reductive stripping of NO adlayers shows little structure sensitivity, mainly manifested in differences in the voltammetric profile for NO_{ads} stripping. This conclusion regarding the apparent structure insensitivity of the reductive stripping of NO adlayers was also supported by the 40 mV decade^{-1} Tafel slopes obtained on different surfaces, which was interpreted in terms of the following EE mechanism:[16]

$$NO_{ads} + H^+ + e^- \leftrightharpoons HNO_{ads} \qquad \text{equilibrium} \quad (1)$$

$$HNO_{ads} + H^+ + e^- \rightarrow H_2NO_{ads} \qquad \text{rds} \quad (2)$$

$$H_2NO_{ads} + 4H^+ + 3e^- \rightarrow NH_4^+ + H_2O \qquad \text{fast} \quad (3)$$

Most importantly, the first two steps of the reaction are assumed to be combined proton−electron transfers, involving hydronium ions from solution. In agreement with the latter assumption, NO_{ads} reduction on Pt(110) (and partly on Pt(111)) occurs at potentials at which the hydrogen coverage is negligible. Additionally, the reductive stripping of NO adlayers on polycrystalline platinum shows a pH dependence that complies with the electrochemical mechanism of NO_{ads} hydrogenation.[20] Note that in mechanism 1−3, N−O bond breaking occurs after the rate-determining step.

The features observed in the voltammetric profile for NO_{ads} reduction were shown to relate to the different reactivity of NO_{ads} species with different surface coordination (i.e., atop, bridge, three-fold-hollow), and not to different (consecutive) steps of an overall process.[17] Chronoamperometric analysis of NO_{ads} reduction on Pt(111) (at all coverages) and Pt(110) (at

* Corresponding author. E-mail: v.rosca@tue.nl.

10.1021/jp052961b CCC: $30.25
Published on Web 08/13/2005

subsaturation coverages) pointed to important lateral (repulsive) interactions between reacting NO species and the apparent first-order kinetics of the overall process.[18] From chronoamperometric reduction of a (nearly) saturated NO adlayer on Pt(110) in perchloric acid (NO coverage of ca. 1 ML), however, we deduced second-order kinetics and a very low Tafel slope of ca. 19 mV decade^{-1} (implying the first three electron/proton transfers to be at equilibrium). The second-order kinetics was interpreted in terms of the necessity of a free neighboring site for breaking the N−O bond, which is only scarcely available at high initial coverage.

The above results make a detailed examination of the mechanism of NO reduction on Pt(100) particularly interesting. In ultrahigh vacuum (UHV), NO has been reported to adsorb in only one position: a site between bridge and atop sites.[21,22] Furthermore, Pt(100) surface is known to be exceptionally active for breaking the N−O bond under UHV conditions,[23] in contrast to Pt(111) and Pt(110). One would expect these factors to be reflected in the kinetics of NO_{ads} reduction on Pt(100) in an electrochemical environment as well.

The adsorption and electrochemical reactions of NO on Pt-(100) have been recently addressed in a number studies.[2,4,5,7,8,24] The NO adsorption on Pt(100) under electrochemical conditions was shown to be quite similar to NO adsorption under UHV conditions, as deduced from in-situ infrared measurements.[10] Most noticeable from a mechanistic point of view is the study by Rodes et al.,[8] who investigated NO adsorption and reactivity in acidic, neutral, and alkaline media. The authors suggested ammonia as the main product of NO_{ads} reduction on Pt(100). The NO_{ads} oxidation was shown to give various products, depending on pH. From a charge analysis applied to the reductive voltammetry of saturated NO adlayers in acidic media, the saturation coverage of nitric oxide was estimated to be ca. 0.5 ML. However, a detailed mechanism for NO_{ads} reduction on Pt(100) in an electrochemical environmental was not proposed.

In this contribution, we present results of a combined voltammetric, in-situ infrared, and on-line mass spectrometric study of the electrocatalytic reduction of NO_{ads} on the Pt(100)-(1×1) surface. We aim at formulating a mechanism for NO_{ads} reduction at this surface, including the effect of anion (co)-adsorption, surface defects, and coverage. Furthermore, we present experimental data on the reduction and oxidation of hydroxylamine on Pt(100), which, we believe, are relevant for a better understanding of the mechanism of NO reduction. We will also provide a comparison of the electrocatalytic reduction of NO_{ads} on Pt(100) with the other two low-index surfaces, Pt-(111) and Pt(110).

2. Experimental Section

The H_2SO_4 and $HClO_4$ working solutions were prepared from their respective concentrated acids (Suprapur, Merck) and ultrapure water (Millipore MilliQ system, 18.2 MΩ cm, less than 3 ppb total organic carbon) or doubly distilled deuterium oxide (Uvasol, Merck, deuteration degree min. 99.9%).

Two types of single-crystal platinum electrodes were used. Bead-type single-crystal platinum electrodes, prepared by Clavilier's method,[25] were used for most of the electrochemical measurements. For in-situ infrared measurements, commercial platinum disk electrodes of 10 mm diameter were used (oriented within 1°, Surface Preparation Laboratory, Zaandam, The Netherlands). Before each experiment, the working electrode was flame-annealed, cooled to room temperature in an Ar:H_2 (3:1) gas mixture, and transferred to the electrochemical cell under the protection of a droplet of deoxygenated ultrapure water.

Electrochemical measurements were performed in a single-compartment three-electrode glass cell, using a computer-controlled potentiostat (AutoLab-PGSTAT20, Eco Chemie, Utrecht, The Netherlands). The cell contained a small movable glass spoon,[26] which contained a diluted $NaNO_2$ (ca. 0.1 mM in 0.1 M perchloric or sulfuric acid) solution. Immersion of the working electrode in the nitrite-containing solution results in the formation of a subsaturated or a saturated (depending on the immersion time) NO adlayer.[2] This procedure allows NO dosing under an inert (argon) atmosphere at open circuit potential and, thus, avoids the use of gaseous NO. In the case of in-situ infrared experiments, NO adlayers were generated in a similar way: immersion of the working electrode in a separate solution of nitrite was followed by washing of the electrode with doubly distilled deuterium oxide and subsequent transfer of the electrode to the spectroelectrochemical cell. The cell and the other glassware were cleaned by boiling in a 1:1 mixture of concentrated nitric and sulfuric acid, followed by repeated boiling with ultrapure water. A coiled platinum wire served as counter electrode. In $HClO_4$ solutions, the reference electrode was an internal reversible hydrogen electrode (RHE). In H_2SO_4 solutions, a saturated mercury−mercury sulfate ($Hg|Hg_2SO_4|K_2SO_{4(sat)}$) electrode, connected via a Luggin capillary, was used as a reference. However, all potentials are quoted versus the RHE. Before each experiment, all solutions were deoxygenated by purging with pure (N50) argon.

The in-situ Fourier transform infrared reflection−absorption spectroscopy (FTIRRAS) measurements were performed under external reflection conditions. The Fourier transform infrared spectrometer was a Brüker IFS113V, equipped with a narrow-band MCT detector. The design of the spectroelectrochemical cell closely resembles that described elsewhere.[27] The cell featured a prismatic CaF_2 transmission window beveled at 60°. Five hundred interferograms were collected at each potential. The spectral resolution was 8 cm^{-1}. The reflectance spectra were calculated as $(R - R_0)/R_0$, where R and R_0 are the reflectance at the sample and the reference potential, respectively. Therefore, the $(R - R_0)/R_0$ ratio gives negative bands for species that are formed and positive bands for species that are consumed at the sample potential, as compared to the reference potential.

The on-line electrochemical mass spectrometry (OLEMS) measurements were performed using a Balzers Quadrupole (QMS 200) mass spectrometer. A Leybold turbo molecular pump together with a Leybold trivac D4B pre-pump assured a pressure lower than 5×10^{-6} mbar. The connection between the mass spectrometer and the cell was established through a steel capillary connected to a glass tube onto which a polyetheretherketon (PEEK, San Diego Plastics, Inc., National City, CA) holder was attached. The inlet of the PEEK holder (ca. 0.6 mm diameter) contained a porous Teflon membrane (pore size 10 μm, Mupor Limited, Scotland, UK). This tip inlet can be placed at 10−20 μm from the electrode surface using a specially designed positioning system. Because of a small surface area of the inlet and, therefore, the small amount of volatile products and solvent entering the tip, differential pumping during measurement is not necessary, thus resulting in a better sensitivity. Before each experiment, the tip (holder + membrane) and the glass tube, which supports the tip, were cleaned by immersion in concentrated chromic acid for ca. 1 h, followed by a thorough rinsing with ultrapure water and then boiling in ultrapure water for ca. 20 min. The proximity of the

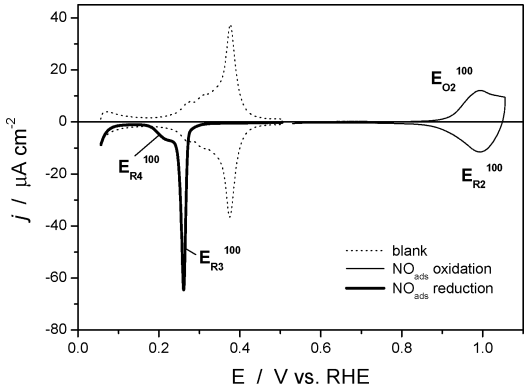

Figure 1. Voltammetry of nitric oxide adlayers on Pt(100) in 0.5 M H_2SO_4. Bold solid line − reductive stripping of a saturated NO adlayer (at 2 mV s^{-1}). Solid line − reversible oxidation of a saturated NO adlayer (at 10 mV s^{-1}). Dotted line − Pt(100)-(1 × 1) blank voltammetry at 10 mV s^{-1}.

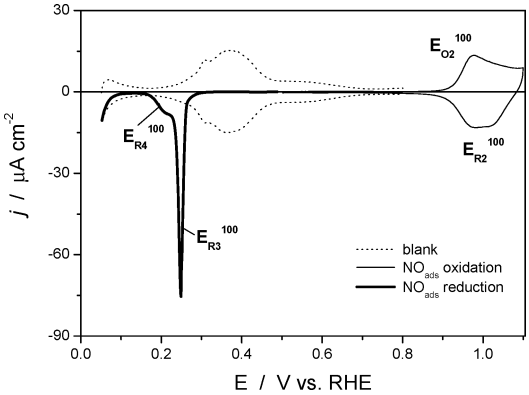

Figure 2. Voltammetry of nitric oxide adlayers on Pt(100) in 0.5 M $HClO_4$. Bold solid line − reductive stripping of a saturated NO adlayer (at 2 mV s^{-1}). Solid line − reversible oxidation of a saturated NO adlayer (at 10 mV s^{-1}). Dotted line − Pt(100)-(1 × 1) blank voltammetry at 10 mV s^{-1}.

tip does not affect the cleanliness of the electrode surface, as deduced from the blank voltammetry. A detailed description of the setup will be published elsewhere.[28]

The surface order and cleanliness of the working electrodes were checked before each experiment by recording the so-called blank cyclic voltammograms and their comparison to the standard voltammetric profile for the Pt(100)-(1 × 1) surface reported elsewhere.[29−31]

3. Results and Data Analysis

3.1. Electrocatalytic Reduction of Adsorbed Nitric Oxide.

3.1.1. Stripping Voltammetry of Saturated NO Adlayers. Figure 1 illustrates the electrochemical reactions of a saturated NO adlayer on Pt(100) surface in sulfuric acid. The saturated NO adlayer is electrochemically stable in a wide potential region between ca. 0.3 and 0.9 V. In this range of potentials, the voltammetric profile shows very low (charging) current densities. At the same time, the hydrogen and the (bi)sulfate adsorption/desorption states in the 0.3−0.45 V region (see the dotted line) are essentially blocked. The voltammetric profile for the reductive stripping of a saturated NO adlayer (bold solid line) contains two characteristic features: a sharp peak E_{R3}^{100} at ca. 0.26 V and a shoulder E_{R4}^{100} at more negative potentials. In perchloric acid (Figure 2), the voltammetric profile for the reductive stripping of a saturated NO adlayer is virtually identical to that in sulfuric acid, thus indicating no effect of anion (co)adsorption.

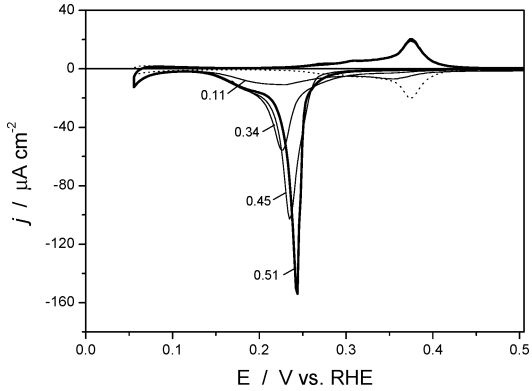

Figure 3. The effect of NO coverage on the voltammetric profile for the reductive stripping of NO adlayers. Experimental conditions: 0.5 M H_2SO_4; starting potential 0.5 V; potential scan rate 5 mV s^{-1}. Numbers indicate the corresponding NO coverage. The dotted line represents the Pt(100) blank voltammetry.

The saturated NO adlayers can be oxidized reversibly (solid line, peaks E_{O2}^{100} and E_{R2}^{100}) both in sulfuric and in perchloric acid, provided the upper potential limit is not higher than 1.1 V and the potential scan rate is not lower than 5 mV s^{-1}. Although chemically reversible, the electrochemical oxidation of a saturated NO adlayer seems to be a complex process: the in-situ infrared data by Rodes et al.[8] suggest that in acidic media the oxidized NO adlayer consists of a mixture of adsorbed nitrito and nitro species, while in alkaline media dissolved nitrite appears to be the main product.

3.1.2. Product of Reduction of Adsorbed NO. Continuous reduction of NO at polycrystalline platinum in acidic solution yields nitrous oxide (and molecular nitrogen) at moderately reductive potentials, while at highly reductive potentials hydroxylamine and ammonia are the products.[19] Importantly, the presence of NO in solution is necessary for the formation of nitrous oxide (and molecular nitrogen) and, therefore, is crucial for N−N condensation.[20] As for the products of NO_{ads} reduction on Pt(100), formation of nitrous oxide may be ruled out, as our in-situ infrared data on the reduction of NO_{ads} show no sign of the formation of nitrous oxide (the N−O and N−N stretching modes at ca. 1285 and ca. 2230 cm^{-1}, respectively), which is in agreement with the above mechanism. Furthermore, OLEMS data to be presented below show no formation of any gaseous products for the reductive stripping of a NO adlayer. Rodes et al. provided spectroscopic data, which strongly suggested ammonia as the main product of NO_{ads} reduction, although not sufficient for ruling out the formation of some hydroxylamine. These authors did not observe N_2O formation in their FTIR experiments. Furthermore, the reductive stripping of a saturated or subsaturated NO adlayer at a sufficiently low scan rate (10 mV s^{-1} or lower) results in a complete recovery of the blank voltammogram, as deduced from the subsequent positive going scan (see, for example, Figure 3). This excludes formation of considerable amounts of an electrochemically active product, that is, hydroxylamine. Pulling these arguments together, ammonia is indeed the main product of the reductive stripping of NO adlayers on Pt(100), similarly to NO_{ads} reduction on Pt-(111) and Pt(110).[17]

3.1.3. NO Coverage and Its Effect on Voltammetric Response. The coverage of the saturated NO adlayer, estimated from a charge analysis proposed elsewhere[4] and assuming ammonia as the main product, lies between ca. 0.5 and 0.52 ML both in sulfuric and in perchloric acid. The experimental reduction charge for the stripping of saturated NO adlayers gives values between 710 and 740 $\mu C\ cm^{-2}$ (before correction for hydrogen

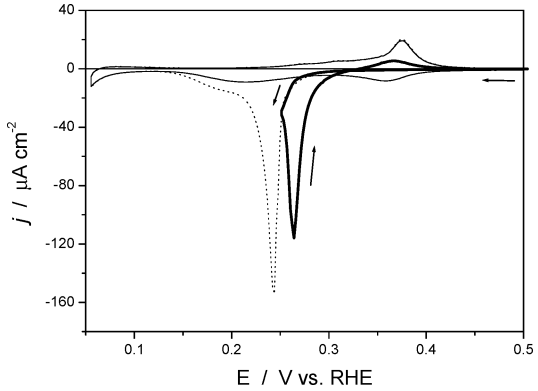

Figure 4. Partial stripping of a saturated NO adlayer (bold solid line) and the voltammetric profile recorded in the subsequent potential cycle (solid line). The dotted line represents the voltammetric profile for a complete stripping of a saturated NO adlayer. Experimental conditions: 0.5 M H_2SO_4; starting potential 0.5 V; potential scan rate 5 mV s^{-1}.

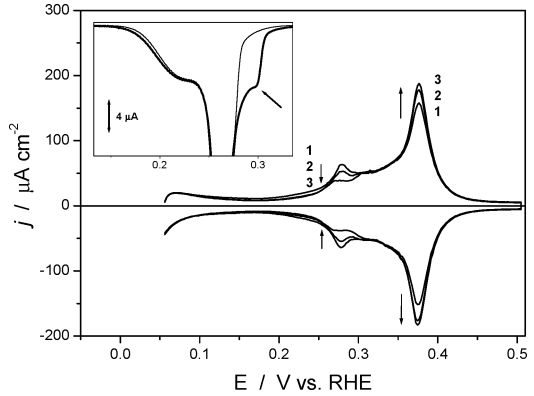

Figure 5. The effect of repeated consecutive deposition and reductive stripping of the saturated NO adlayers on the blank voltammetry of Pt(100). Curve 1 corresponds to the initial blank voltammetry. Curves 2 and 3 correspond to the Pt(100) blank voltammogram recorded after the first and third cycles of deposition and reductive stripping (at 2 mV s^{-1}) of saturated NO adlayers. Experimental conditions: 0.5 M H_2SO_4; potential scan rate 50 mV s^{-1}. The inset shows the voltammetry of the first (bold solid line) and the third (solid line) NO adlayer stripping at 2 mV s^{-1}.

adsorption) for integration between 0.5 and 0.1 V. These values of the reduction charge and the corresponding coverage values agree well with estimations by the Alicante group.[4,7,8] The value of ca. 0.5 ML for the saturation coverage of NO under electrochemical conditions would coincide with the value for NO saturation coverage on Pt(100)-(1 × 1) surface under UHV conditions, as reported by different groups.[21,22,32] In more recent UHV studies, lower values for the NO saturation coverage were reported, particularly in connection with the possibility of NO dissociation even at room temperature.[33−35] The issue of NO dissociation under UHV and electrochemical conditions and the related issue of the saturation coverage and the structure of NO adlayer will be addressed in some detail in the Discussion section.

Figures 3 shows the effect of the initial NO_{ads} coverage on the voltammetric profile for the reductive stripping of nitric oxide adlayers in sulfuric acid. In perchloric acid, the effect of the initial NO coverage is quite similar (data not shown). Decrease of the initial coverage brings about a slight positive shift and attenuation of the main peak position (E_{R3}^{100}), while feature E_{R4}^{100} seems to remain unchanged at moderate to high coverages. Note that at subsaturated coverage, the reduction of NO adsorbate seems to start slightly (ca. 50 mV) more positively. The voltammetric profile corresponding to the reductive stripping of ca. 0.1 ML of NO_{ads} exhibits only one broad feature in the potential region between ca. 0.3 and 0.15 V.

The voltammetric profile corresponding to the reductive stripping of a saturated NO adlayer can be represented reasonably well as a combination of two overlapping Voigtian peaks. The ratio of the area (charge) under the sharp peak E_{R3}^{100} and that under the broad feature E_{R4}^{100} (Q_{R3}/Q_{R4}) changes from ca. 2:1 at saturation to ca. 1:1 at ca. 0.34 ML, thus indicating an apparent attenuation of feature E_{R3}^{100} and not of feature E_{R4}^{100} with decreasing coverage in the 0.5−0.3 ML range.

The above data suggest that the reduction features E_{R3}^{100} and E_{R4}^{100} can be tentatively ascribed to the reduction of NO adsorbates having different reactivity, rather than to consecutive steps of the same reaction. We shall return to this issue again when discussing the results of the Tafel slope analysis of the two reduction features.

Figure 4 shows results corresponding to partial stripping of a saturated NO adlayer. In this experiment, the first, negative-going, run was reversed at ca. 0.26 V (the bold solid line). The subsequent positive-going scan shows a reduction peak at potentials ca. 50 mV more positive than it should have appeared if the potential run was not reversed (compare the bold solid line and the dotted line). First, this result seem to be in good agreement with the autocatalytic nature of NO reduction on Pt(100), known from the UHV studies.[36] Second, the strong hysteresis observed also indicates that the NO reaction on platinum is chemically irreversible at the initial stages of the reaction. Note that such a hysteresis was not observed for partial stripping of NO adlayers on Pt(111) and Pt(110).[17]

3.1.4. Effect of Surface Defects. To elucidate the effect of the surface defects, we have examined the reductive stripping of the saturated NO adlayers at Pt(100) electrode with different degrees of the surface order (Figure 5). The order of the electrode surface can be assessed from the blank voltammetry. The cyclic voltammogram corresponding to a well-ordered Pt(100)-(1 × 1) surface in contact with sulfuric acid is shown in Figure 1 (the dotted line), as deduced from combined voltammetric and LEED[31] or STM[37] studies. More specifically, the magnitude of the peak at ca. 0.38 V is a measure of the long-range order of the surface.[31,38] In our experiments, the height of this peak was typically 200 μA cm^{-2} or higher for cyclic voltammetry measurements at 50 mV s^{-1}. The surface defects appear for an electrode cooled in air or even in the presence of traces of oxygen,[39] or can be generated by the potentiodynamic cycling[29] (see also Figure 6 and its caption for details). The development of defects is reflected in a substantial current increase in the 0.05−0.25 V range, which seems to indicate increasing contribution from (111) sites, and a decrease of the adsorption state around 0.38 V. The sharp peaks at ca. 0.28 V (Figure 6) should relate mainly to (100) × (111) step defects.[31,38]

Turning now to the effect of the surface defects on the reduction of NO_{ads}, the presence of the defect sites, which give rise to the pair of peaks at ca. 0.28 V (Figure 5), is reflected in the appearance of a preshoulder to the main peak of the NO_{ads} stripping (see the inset of Figure 5). Figure 6 shows the blank CVs for a well-ordered Pt(100)-(1 × 1) (bold solid line) as compared to Pt(100) surfaces with a different level of the surface disorder. Figure 7 illustrates the stripping voltammetry of saturated NO adlayers from those surfaces. Most noticeably, the sharp peak E_{R3}^{100} shifts toward positive potentials and loses its intensity with shoulders evolving at negative and positive potentials. The surface defect sites appear to be more active

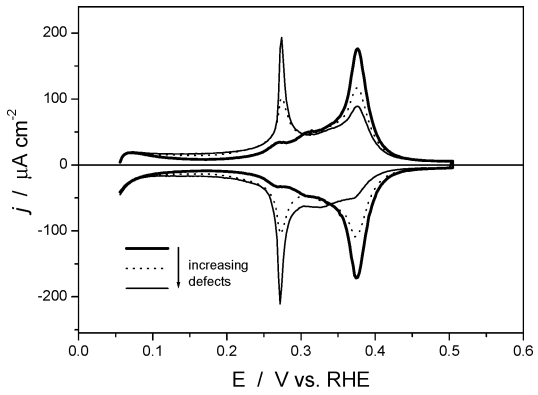

Figure 6. Blank cyclic voltammetry of Pt(100)-(1 × 1) surface (bold solid line) as compared to disordered Pt(100) surfaces. Dotted and solid lines correspond to the cyclic voltammograms resulted from an initially well-ordered surface after 15 and 50 potential cycles, respectively, between 0.06 and 0.9 V at 20 mV s^{-1}.

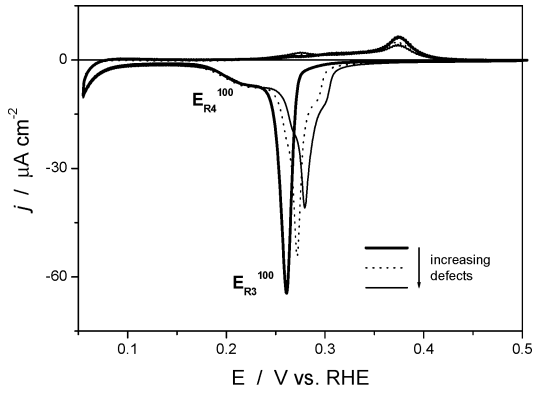

Figure 7. Stripping voltammetry for the electrochemical reduction of saturated nitric oxide adlayers on Pt(100) with different degrees of the surface disorder. Experimental conditions: 0.5 M H_2SO_4; starting potential 0.5 V; potential scan rate 2 mV s^{-1}. The corresponding initial blank voltammetric profiles are presented in Figure 6.

sites for NO reduction, as compared to the sites on the (100) terrace, although the effect is quite moderate.

Remarkably, consecutive deposition and stripping of the saturated NO adlayer result in a gradual decrease of the current contribution around 0.28 V and a simultaneous increase of the intensity of the peaks at ca. 0.38 V in the blank voltammetry, which are characteristic for the adsorption/desorption processes on (100) terraces (Figure 5). Moreover, NO adsorption and reductive stripping bring about a considerable ordering, although not a complete recovery, of even strongly disordered Pt(100) surfaces, such as the surfaces voltammograms of which are shown in Figure 6. This result indicates that NO adsorption and/or NO reductive stripping can effectively extend the (100)-(1 × 1) domains at the expense of certain surface defects, apparently (100) × (111) step sites. This apparent smoothening of the surface can be tentatively assigned to the quasi-hexagonal reconstruction of small (1 × 1) domains (islands) (although, unlikely the extended (100) terraces) on the surface, and the subsequent lifting of the reconstructed domains by NO adsorption resulted in formation of more extended (1 × 1) domains.

3.1.5. Tafel Slope Analysis. Figure 8 shows the results of the Tafel slope analysis of the reduction features $E_{R3}{}^{100}$ and $E_{R4}{}^{100}$ in perchloric (A) and sulfuric acid (B), respectively. As shown elsewhere,[40,41] the peak position (E_p) versus logarithm of the scan rate (υ) graph allows determination of the Tafel slope for surface-confined processes, both for first- and for second-order kinetics. The peak position of the feature $E_{R4}{}^{100}$ was obtained

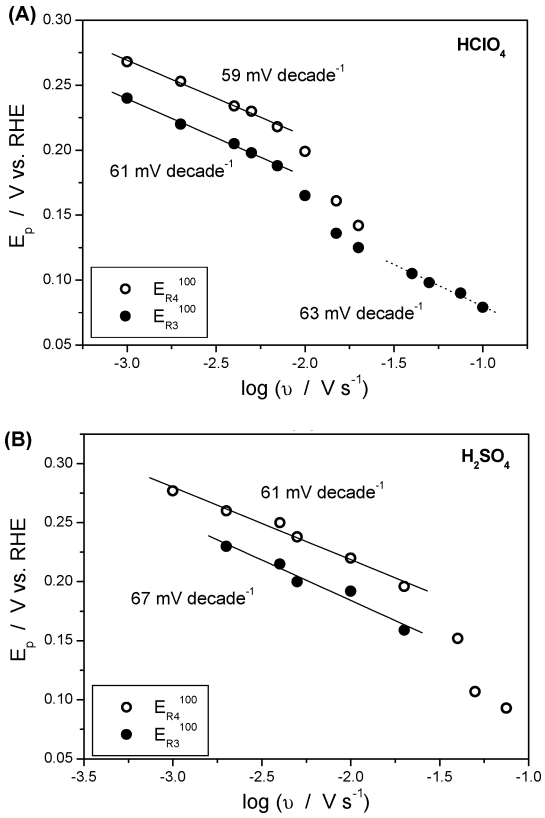

Figure 8. Tafel slope analysis of the voltammetric features E_{R3} and E_{R4} in perchloric (A) and sulfuric (B) acid. Experimental conditions: 0.5 M $HClO_4$ or 0.5 M H_2SO_4; saturated NO adlayer; starting potential 0.5 V. The numbers indicate the slope of the corresponding least-squares linear regression lines.

from deconvolution of the voltammetric profile corresponding to the reductive stripping of a saturated NO adlayer into two Voigtians. In the scan rate region between approximately 1 and 20 mV s^{-1}, the $E_p - \log(\upsilon)$ dependences for the reduction peaks $E_{R3}{}^{100}$ and $E_{R4}{}^{100}$ show good linearity for experiments in both sulfuric and perchloric acid, with Tafel slopes close to 60 mV $decade^{-1}$. At higher scan rates, the two features overlap even stronger and there is a clear deviation from the initial linearity of the $E_p - \log(\upsilon)$ dependence. Interestingly, for experiments in perchloric acid, we could observe an apparent recovery of the linearity and the slope at higher scan rates (50−100 mV s^{-1}), although only one reduction peak is observed. As an important observation, the reduction features $E_{R3}{}^{100}$ and $E_{R4}{}^{100}$ show similar Tafel slopes, which would rather favor the assumption that these features are related to the reduction of adsorbed NO species having somewhat different reactivity and not to consecutive steps of an overall process.

3.1.6. In-Situ FTIR Measurements. Figure 9 contains the potential difference spectra for the reductive stripping of a saturated NO adlayer on Pt(100). The experiment was started with a saturated NO adlayer at 0.5 V, a potential at which NO_{ads} is (electro)chemically stable. Significantly, the potential dependent band centered between ca. 1620 and 1590 cm^{-1} (N−O stretching mode in NO_{ads} in a position between atop and bridge sites[22]) is not observed at potentials lower than ca. 0.3 V. This does not necessarily mean that there is no NO_{ads} left on the surface: some NO molecules may be still present, but either at a too low coverage to be detected or with an altered orientation, for example, by adopting a configuration similar to the theoretically predicted "side-on" configuration.[42] Note that the broad potential-independent band at ca. 1465 cm^{-1} is most probably

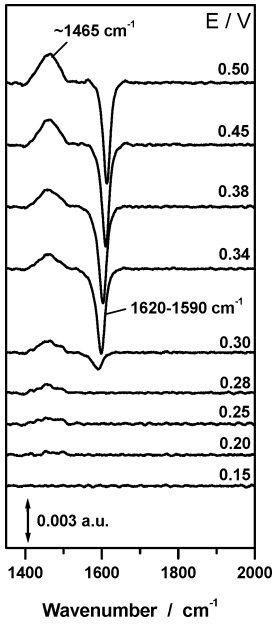

Figure 9. Potential difference infrared spectra for electrochemical reduction of a saturated NO adlayer on Pt(100). Experimental conditions: 0.1 M $HClO_4$ (in D_2O); p-polarized light; reference potential 0.1 V.

related to a solution species, a product of NO_{ads} reduction. (We identify these species as ammonium cations, containing H and D atoms in different ratios. For details on the origin of this feature, see ref 17.) Accordingly, this feature does not show any significant evolution in the potential region in which NO_{ads} is stable. In the potential region in which NO_{ads} is reduced (ca. 0.35−0.20 V), absorption around 1465 cm^{-1} increases with decreasing the potential, corresponding to accumulation of a solution species. This result also indicates that, in agreement with voltammetric results, reduction of all NO_{ads} species requires a potential as low as ca. 0.2 V.

3.2. Electrocatalytic Reduction and Oxidation of Hydroxylamine. In the remaining part of this section, we shall examine the electrochemical transformations of hydroxylamine (HAM) on Pt(100). In our view, the combination of data on hydroxylamine and NO_{ads} reduction is relevant for a better understanding of the mechanism of NO_{ads} reduction, as well as for the mechanism of HAM reduction itself.

3.2.1. Cyclic Voltammetry. Figure 10 shows the voltammetric reduction and oxidation of HAM in sulfuric acid. More specifically, the figure shows the effect of the upper-potential limit (vertex potential) on the negative-going voltammetric profile. In this experiment, the potential cycle was started at ca. 0.06 V and was run in the positive-going direction first. Continuous potential cycling, combined with a gradual increase of the upper potential limit of the cyclic voltammogram, allowed us to follow the appearance and evolution of the features in the negative-going scan (Figure 10). If a sufficiently low potential sweep rate is applied (5 mV s^{-1} or lower), the positive-going sweep shows the same voltammetric profile (as that shown by the bold black line), while the negative-going voltammetric profile changes as a function of the vertex potential.

As an important observation from the above experiment, reversing the potential at ca. 0.3 V (or more positive) results in the appearance of a reduction feature at ca. 0.22 V, which cannot be associated with HAM reduction, but rather with reduction of a product of the HAM partial dehydrogenation.[43] This can be concluded from the much lower currents observed in the 0.1−0.25 V region in the positive-going scan, thus indicating a

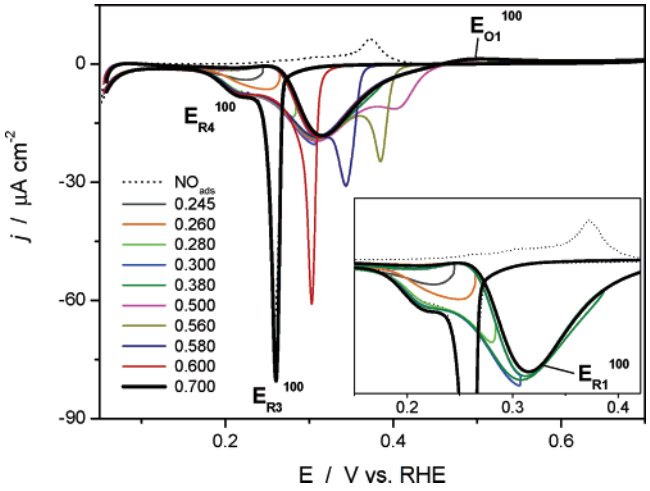

Figure 10. Voltammetry of hydroxylamine on Pt(100). See text for details on the potential program. Experimental conditions: 0.5 M H_2SO_4 + (1 × 10^{-2} M) NH_2OH; starting potential 0.05 V; potential scan rate 2 mV s^{-1}. Dotted line represents the reductive stripping of a saturated NO adlayer. Numbers indicate the upper potential limit of the corresponding voltammogram.

low "direct" HAM reduction reactivity in this potential region. The position and the height of the reduction feature observed in the negative-going scan at ca. 0.22 V do not depend on the HAM concentration[43] or the vertex potential (for potentials higher than ca. 0.3 V). Significantly, the position and height of this feature appear to be identical to those of the feature E_{R4}^{100}, which is characteristic to the NO_{ads} stripping profile (Figure 10, the dotted line). The above observations suggest that HAM reduction, which seems to involve initial partial dehydrogenation,[43] and NO_{ads} reduction proceed through the same intermediate.

The reduction feature E_{R1}^{100} (see the inset of Figure 10) corresponds to HAM reduction to ammonia. Accordingly, we did not observe formation of any gaseous products in this region by both infrared and mass spectrometry measurements (see sections 3.2.2 and 3.2.3). The oxidation feature E_{O1}^{100} corresponds to HAM oxidation to adsorbed nitric oxide. Figure 10 shows that a saturated NO adlayer can be formed provided a sufficiently long polarization at ca. 0.6 V or higher is applied. Accordingly, the negative-going part of the CV reversed at 0.7 V shows a profile identical to that for the reductive stripping of a saturated NO adlayer.

Note a sharp transition from HAM reduction to ammonia (Figure 10, feature E_{R1}^{100}) to HAM oxidation to NO_{ads} (Figure 10, feature E_{O1}^{100}). We would not exclude the possibility of simultaneous occurrence of the two processes around 0.45 V. In any case, these two processes sharing an intermediate would be a reasonable explanation for the observed voltammetric profile. We shall propose a candidate for such an intermediate in the Discussion section.

Intriguingly, Figure 10 indicates that the negative-going part of the CVs reversed below ca. 0.6 V shows, along with features E_{R1}^{100} and E_{R4}^{100}, a reduction peak, the height and position of which depend on the upper potential limit. The higher is the upper potential limit, the more positive is the peak position and the more intensive is the peak. Because features E_{O1}^{100} and E_{R3}^{100} correspond to the formation and reductive stripping, respectively, of NO_{ads}, it would be logical to assume that this reduction peak corresponds to the reductive stripping of a subsaturated NO adlayer. At the same time, note that we did not observe any considerable positive shift of the E_{R3}^{100} feature

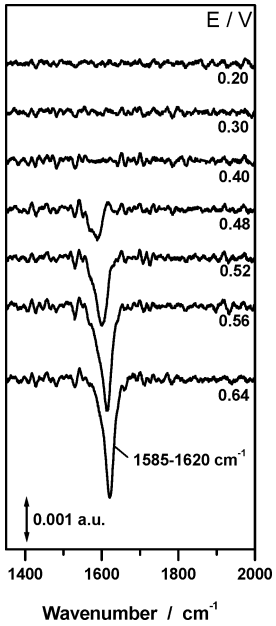

Figure 11. Potential difference infrared spectra for electrochemical oxidation of hydroxylamine at Pt(100) surface. Experimental conditions: 0.1 M $HClO_4$ + (1×10^{-3} M) NH_2OH (in D_2O); p-polarized light; reference potential 0.1 V.

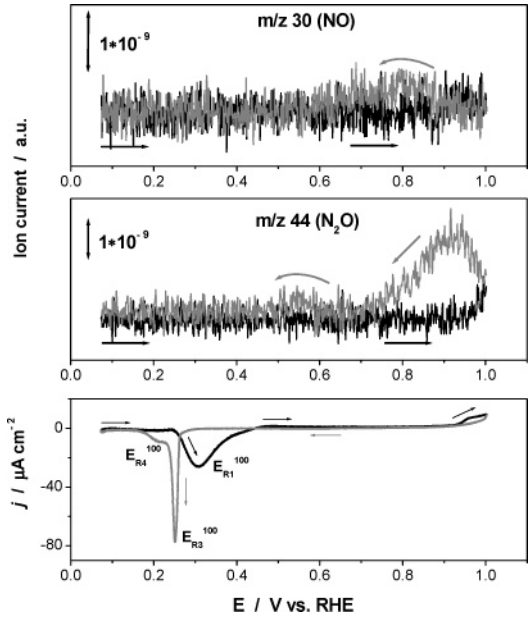

Figure 12. Results of the on-line electrochemical mass-spectrometry measurements for the electrochemical reactions of hydroxylamine. Experimental conditions: 0.5 M H_2SO_4 + (20×10^{-3} M) NH_2OH; starting potential 0.05 V; potential scan rate 2 mV s^{-1}. Black line − positive-going scan; gray line − subsequent negative-going scan.

with decreasing NO coverage (for NO adlayers formed by NO dosing from nitrite, see Figure 3). Therefore, we assume that the structure and the reactivity of the (subsaturated) NO adlayer formed as a result of HAM oxidation and that formed upon NO dosing from nitrite solution differ, although their structures are identical at saturation. A definite interpretation of the evolution of the voltammetric profile described in this paragraph is difficult, because the structure of the subsaturated NO adlayer is unclear.

3.2.2. In-Situ FTIR Measurements. The above interpretation of the oxidation feature E_{O1}^{100} is corroborated by the in-situ infrared data presented in Figure 11. This figure contains a series of the potential difference spectra, which show a potential-dependent negative-going band (corresponding to the accumulation of a product) centered between ca. 1586 and 1620 cm^{-1}. We assign this band to the N−O stretching mode of NO molecules adsorbed on (100) terraces, in agreement with previous in-situ infrared studies by different groups.[4,10] As the most important message of this figure, NO_{ads} can be detected at ca. 0.5 V or more positive potentials, which clearly indicates that the feature E_{O1}^{100} corresponds to HAM oxidation to NO_{ads}. Finally, in our infrared experiments, we did not observe formation of nitrous oxide (the N−O and N−N stretching modes at ca. 1285 and ca. 2230 cm^{-1}, respectively).

3.2.3. On-Line Mass Spectrometry. Figure 12 shows the results of the OLEMS measurements of HAM electrochemical transformations at the Pt(100) surface. No gaseous products are observed in the potential region between ca. 0.05 and 0.9 V during the positive-going sweep (we also monitored *m*/*z* 26 (N_2) and *m*/*z* 46 (NO_2)). This result strongly suggests that the reduction feature E_{R1}^{100} corresponds to HAM reduction to ammonia and that this process, although involving a partial dehydrogenation of HAM, is not accompanied by side (e.g., N−N condensation) reaction. Furthermore, no gaseous products appear to accompany HAM oxidation to NO_{ads} (the oxidation feature E_{O1}^{100} at ca. 0.5 V), in contrast to HAM oxidation to NO_{ads} on Pt(111) and Pt(110) surfaces, which is accompanied by the formation of some N_2O at potentials corresponding to the formation of a subsaturated NO adlayer.[28,43] The (saturated) NO adlayer blocks sites for further HAM oxidation, acting as a catalyst poison. Therefore, low current densities are observed in the positive-going scan (Figure 12, the solid black lines). N_2O formation and, to a smaller extent, NO formation are observed in the positive-going scan starting at ca. 0.9 V and in the subsequent negative-going scan in the 1−0.7 V potential range (Figure 12, the solid gray lines). The formation of nitrous oxide at highly oxidative potentials (around 0.9 V) is most probably related to a reaction between the nitrite, resulting from NO_{ads} oxidation, and HAM. Accumulation of some NO in solution may be tentatively assigned to (i) partial desorption of NO adlayer and/or (ii) (homogeneous) decomposition of nitrite to NO.

As shown above, HAM oxidation in the potential window between ca. 0.45 and 0.6 V appears to result in formation of a NO adlayer. The negative-going scan in Figure 12 (the solid gray line) shows a profile virtually identical to the one recorded for the reductive stripping of a saturated NO adlayer in the absence of HAM in solution. Furthermore, no gaseous products are observed during the reductive stripping of this NO adlayer, even in the presence of HAM (the potentials region between ca. 0.4 and 0.05 V; Figure 12, solid gray line). This result points again to ammonia as the product of NO_{ads} reduction on the Pt-(100) surface.

4. Discussion

4.1. Saturation Coverage and Structure of NO Adlayer. Studies of NO adsorption on Pt(100) surface under UHV conditions are complicated by a high activity of this surface toward NO dissociation.[23] This high activity is one of the major factors determining the uncertainty in assessing the NO saturation coverage and the structure of NO adlayer on Pt(100) in UHV at room temperature. In earlier UHV studies of NO adsorption on Pt(100), it was generally accepted that at room temperature NO adsorbs molecularly and that the dissociation of NO takes place at temperatures well above 300 K. Although the possibility of NO dissociation on Pt(100) at room temper-

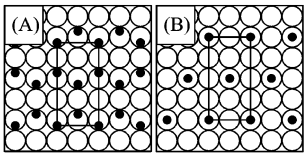

Figure 13. Structural models for saturated NO adlayer on Pt(100)-(1 × 1). Panel A shows a $c(2 \times 4)$ overlayer structure with 0.5 ML coverage, proposed by Yeo et al. (ref 32) as a development of earlier models (refs 45 and 22). Panel B shows a simple $c(2 \times 4)$ overlayer structure with 0.25 ML coverage, as proposed by Song et al. (ref 34).

ature was repeatedly suggested,[33−35] this process seems to be quite sluggish (on the order of tens of minutes[44]).

The saturation coverage of 0.5 ML and a $c(2 \times 4)$ overlayer structure (Figure 13A) seem to account well for the LEED,[45] vibrational,[21,22] and the adsorption calorimetric[32] data for NO adsorption on Pt(100) at room temperature. A somewhat lower coverage (ca, 0.4 ML) for the saturation NO adlayer at room temperature was reported by Zemlyanov et al.[46,47] in their combined EELS and TPD studies of NO adsorption and reduction on Pt(100); the authors did not address the structure of the adlayer. More recently, in an STM study, Song et al.[34] proposed a simple $c(2 \times 4)$ overlayer structure corresponding to a coverage of 0.25 ML for the saturation NO adlayer on Pt-(100) at 300 K (Figure 13B). Rienks et al.[35] showed in their synchrotron XPS study that in the temperature range between 250 and 325 K both molecular and dissociative adsorption of NO takes place.

Turning to the coverage estimation under electrochemical conditions, the charge analysis of the stripping voltammetry of the saturated NO adlayer gives a coverage of ca. 0.5 ML, assuming ammonia as the only product of NO_{ads} reduction. This value would be consistent with the formation of a $c(2 \times 4)$ overlayer structure (or whatever the structure of the saturated adlayer is) under electrochemical conditions as well, as proposed in earlier in-situ electrochemical studies.[7,8] The resemblance of the infrared spectra recorded for NO adsorbed on Pt(100) under electrochemical and UHV conditions at room temperature[10,17] supports the assumption of the structural similarity. As an indication of the stability of the molecularly adsorbed NO species, the voltammograms for Pt(100) covered with a saturated NO adlayer show very low and stable (charging) current in a wide potential region between ca. 0.9 and 0.3 V. The "direct" dissociation of NO molecules would result in the formation of adsorbed oxygen-containing species, which would not be stable in the above potential region and would show significant faradaic currents. All together, our experimental data as well as the considerations given above confirm that in an electrochemical environment (acidic media) the NO species are adsorbed molecularly on Pt(100) and the NO saturation coverage is ca. 0.5 ML.

4.2. Mechanism of Reduction of NO_{ads} on Pt(100). The Tafel slope analysis of the reduction features E_{R3}^{100} and E_{R4}^{100} (Figure 8), corresponding to the reductive stripping of a saturated NO adlayer, gives a good linearity of the $E_p-\log(\upsilon)$ dependence. The slopes for both features are close to the theoretical value of 60 mV decade^{-1}, irrespective of the anion (sulfate vs perchlorate). This result indicates that both features correspond to an electrochemical process, in which the first electron (likely accompanied by a proton transfer) is fast (at equilibrium), while the second step is a chemical and rate-determining step. Because the reduction of NO_{ads} on Pt(100) seems to become chemically irreversible at an early stage of the process (Figure 4 and the corresponding discussions) and the breaking of the N−O bond is expected to be facile on Pt(100), we propose the following mechanism for NO_{ads} reduction:

$$NO_{ads} + e^- + H^+ \leftrightharpoons HNO_{ads} \qquad \text{equilibrium} \qquad (4)$$

$$HNO_{ads} + * \rightarrow HN_{ads} + O_{ads} \qquad \text{slow} \qquad (5)$$

$$HN_{ads} + 2e^- + 3H^+ \rightarrow NH_4^+ + * \qquad \text{fast} \qquad (6)$$

$$O_{ads} + 2e^- + 2H^+ \rightarrow H_2O + * \qquad \text{fast} \qquad (7)$$

The overall reaction would then be:

$$NO_{ads} + 5e^- + 6H^+ + * \rightarrow NH_4^+ + H_2O + 2* \qquad (8)$$

Most importantly, we assume here that, similarly to NO reduction in UHV, breaking of the N−O bond (in HNO_{ads}) requires an adjacent free site. The reason HNO and not NOH is suggested as the first intermediate is that gas-phase HNO is about 100 kJ mol^{-1} more stable than gas-phase NOH,[20] although their stability at the surface is admittedly unknown. Interestingly, Zemlyanov et al.,[48] in their combined TPR and HREELS studies, have pointed to the formation of HN_{ads} and H_2N_{ads} species during NO_{ads} reduction on Pt(100)-(1 × 1) at 300 K. Smirnov et al.[49] claimed the existence of chemisorbed HNO during the coadsorption of NO and H on Pt(111) from HREELS experiments. Reactions 6 and 7 are complex processes, which likely involve fast electron/proton transfers. On the other hand, these reactions may still involve catalytic hydrogenation steps, as the electrochemical reduction of NO adlayers occurs at potentials corresponding to significant hydrogen coverage.

Remarkably enough, feature E_{R4}^{100}, characteristic of the NO_{ads} stripping profile, can be also generated in experiments concerning HAM reduction (Figure 10). This observation implies intriguing mechanistic implications for HAM reduction. If feature E_{R4}^{100} indeed corresponds to NO_{ads} reduction to ammonia through HNO_{ads} (or alternatively NOH_{ads}) intermediate, then HAM electroreduction should imply HAM dehydrogenation to HNO_{ads} and its subsequent reduction to ammonia according to reactions 5−7. Note that the HAM oxidation to HNO_{ads} would imply a transfer of two electrons, while HNO_{ads} reduction to ammonia (NH_4^+) requires four electrons. Therefore, the net current would be still negative, in accordance with the experiment. Furthermore, as indicated in the Results and Data Analysis section, existence of a common intermediate (HNO_{ads}) would provide a reasonable explanation for a quite sharp transition (or possibly simultaneous occurrence) from HAM reduction to ammonia to HAM oxidation to NO_{ads} in the 0.4−0.5 V range.

4.3. Comparison to the Mechanism of NO_{ads} Reduction on Pt(111) and Pt(110). The voltammetric features observed in the voltammetric profile for NO_{ads} reduction on Pt(111) and Pt(110) are determined by reaction of NO_{ads} species having different coordination, as discerned from in-situ infrared measurements.[17] Similar analysis is less conclusive for NO_{ads} reduction on Pt(100). Note that (HR)EELS studies[21,48] as well as FTIR[22] studies under UHV conditions (room temperature) indicate a single N−O stretching frequency of NO_{ads} on Pt-(100)-(1 × 1) surface (1600−1640 cm^{-1} region), thus pointing to a single NO adsorption site on (100) terraces at saturation. This adsorption site is usually identified as a position between atop and bridge site, as shown in Figure 13A. In an electrochemical environment, adsorbed NO is also characterized by a single N−O stretching band in the 1590−1620 cm^{-1} range of frequencies, which, however, is not observed at potentials lower

than ca. 0.3 V (Figure 9). Therefore, the two features observed in voltammetric profile for reduction of a saturated NO adlayer cannot not be straightforwardly ascribed to the reaction of NO species having different coordination, which is in contrast to NO_{ads} reduction on Pt(111) and Pt(110).

At the same time, it is important to realize that at saturation coverage a simultaneous reaction of all NO molecules on Pt(100) under UHV conditions or in an electrochemical environmental is very unlikely. This aspect is related to the necessity of a free site for breaking the N−O bond under UHV conditions and assumedly in an electrochemical environment. Therefore, we shall consider the possibility of formation of a quasi-stable surface configurations formed by subsaturated NO adlayer and coadsorbed hydrogen. Existence of such a configuration would imply a different reaction environment and possibly different adsorption geometry for NO adsorbate and, thus, could give rise to a second reduction feature.

Comparing the mechanisms of the electrocatalytic reduction of NO_{ads} on Pt(111), Pt(110),[16,18] and Pt(100) (present work), the process appears to be mechanistically structure sensitive, although the main product is the same at all three surfaces, ammonia. More specifically, on Pt(110) and Pt(111), breaking of the N−O bond is preceded by two to three concerted electron−proton transfers at equilibrium (Tafel slope of 40 mV decade^{-1} or even lower[16,18]), while on Pt(100) the N−O bond breaking seems to occur after the first electron−proton transfer (Tafel slope of 60 mV decade^{-1}). The more facile breaking of the N−O bond on Pt(100), as compared to the other two surfaces, is in remarkable concordance with a similar trend observed in UHV: Pt(100) is the only low-index surface at which the dissociative adsorption of NO occurs. At the same time, electrochemical hydrogenation followed by the N−O bond breaking seems to provide an energetically more favorable route for NO_{ads} reduction on Pt(100), as compared to a direct breaking of the N−O bond. Furthermore, reactions 4−7 exclude formation of hydroxylamine as a result of NO_{ads} reduction on Pt(100).

Finally, as shown in the Results and Data Analysis section, the surface defects appear to be more active sites for NO reduction, as compared to the sites on the (100) terrace, although the effect is moderate. Lack of a considerable effect of the step density on the electrocatalyst activity was also observed for NO_{ads} reduction on Pt(111), Pt(110), and a series of Pt-[*n*(111) × (111)] stepped surfaces. This result is, in fact, expected, because the activity of platinum surfaces toward NO_{ads} reduction seems to be determined by the coordination (linear versus multiple bonding) of NO adsorbate, and not to specific reaction sites, for example, low-coordination metal atoms.

5. Summary

We have used voltammetry, in-situ infrared spectroscopy, and on-line mass spectroscopy to study the mechanism of the electrocatalytic reduction of adsorbed nitric oxide on Pt(100)-(1 × 1) as well as some related mechanistic aspects of hydroxylamine transformations. We have examined the effect of surface defects, NO coverage, and the nature of the supporting electrolyte (sulfate vs perchlorate).

The voltammetric profile for the electrochemical reduction of a saturated NO adlayer exhibits two features, which were tentatively ascribed to reactions of NO species having different reactivity. Ammonia was shown to be the main product of NO_{ads} reduction on Pt(100), most probably irrespective of the coverage. The surface defects, in particular (100) × (111) steps, render the Pt(100) surface a higher activity toward NO_{ads} reduction, although the effect is moderate. The reactivity of the saturated NO adlayer on Pt(100) does not seem to be affected by the nature of the anion. There is also a small effect of the NO_{ads} coverage: the reduction of subsaturated NO adlayers starts at more positive potentials (ca. 50 mV).

The Tafel slope analysis of the features appearing in the voltammetric profile for the reductive stripping of a saturated NO adlayer gives values of ca. 60 mV decade^{-1}, irrespective of the nature of anion. This value of the Tafel slope was interpreted in terms of an EC mechanism, in which the first electron/proton transfer is at equilibrium, while the second reaction step is a chemical rate-determining step. This chemical step is assumed to involve the N−O bond breaking in HNO_{ads} intermediate and is postulated to require a free neighboring site.

When comparing NO_{ads} reduction on Pt(100) to NO_{ads} reduction on Pt(110) and Pt(111), breaking of the N−O bond on Pt(100) appears to occur at an earlier stage of the reaction. This result leads to the following observations. First, the mechanism of NO_{ads} reduction on platinum depends on the surface structure, although the main reaction product is still the same, ammonia. Second, despite comparable overall activities of the three surfaces toward NO_{ads} reduction, Pt(100) is still the most active in breaking the N−O bond, which is in interesting agreement with the similar trend observed under UHV conditions.

The mechanism proposed for the electrocatalytic reduction of NO adsorbate on Pt(100) seems to provide a framework for explaining the electrocatalytic transformations of HAM at the same surface. As suggested in our previous studies,[43] the electrocatalytic reduction of HAM is likely to proceed through partial dehydrogenation of HAM. In this study, we further developed that idea, and, on the basis of the mechanism for NO_{ads} reduction proposed here, we suggest the HNO_{ads} (or alternatively NOH_{ads}) to be the intermediate appearing both in HAM reduction/oxidation and in NO_{ads} reduction.

Acknowledgment. This work was supported by a grant from The Netherlands Organization for Scientific Research (NWO).

References and Notes

(1) Plieth, W. J. In *Encyclopedia of Electrochemistry of the Elements*; Bard, A. J., Ed.; Marcel Dekker: New York, 1978; p 422.
(2) Rodes, A.; Gomez, R.; Orts, J. M.; Feliu, J. M.; Perez, A.; Aldaz, A. *J. Electroanal. Chem.* **1993**, *359*, 315.
(3) Ye, S.; Kita, H. *J. Electroanal. Chem.* **1993**, *346*, 489.
(4) Gomez, R.; Rodes, A.; Orts, J. M.; Feliu, J. M.; Perez, J. M. *Surf. Sci.* **1995**, *342*, L1104.
(5) Rodes, A.; Gomez, R.; Orts, J. M.; Feliu, J. M.; Perez, A.; Aldaz, A. *Langmuir* **1995**, *11*, 3549.
(6) Villegas, I.; Gomez, R.; Weaver, M. J. *J. Phys. Chem.* **1995**, *99*, 14832.
(7) Rodes, A.; Gomez, R.; Perez, A.; Feliu, J. M.; Aldaz, A. *Electrochim. Acta* **1996**, *41*, 729.
(8) Rodes, A.; Climent, V.; Orts, J. M.; Perez, J. M.; Aldaz, A. *Electrochim. Acta* **1998**, *44*, 1077.
(9) Momoi, K.; Song, M. B.; Ito, M. *J. Electroanal. Chem.* **1999**, *473*, 43.
(10) Weaver, M. J.; Zou, S.; Tang, C. *J. Chem. Phys.* **1999**, *111*, 368.
(11) Weaver, M. J. *Surf. Sci.* **1999**, *437*, 215.
(12) Zang, Z.-H.; Wu, Z.-L.; Yau, S.-L. *J. Phys. Chem. B* **1999**, *103*, 9624.
(13) Zou, S.; Gomez, R.; Weaver, M. J. *J. Electroanal. Chem.* **1999**, *474*, 155.
(14) Casero, E.; Alonso, C.; Martin-Gago, J. A.; Bogatti, F.; Felici, R.; Renner, R.; Lee, T.; Zegenhagen, J. *Surf. Sci.* **2002**, *507−510*.
(15) Alvarez, B.; Rodes, A.; Perez, J. M.; Feliu, J. M.; Rodriguez, J. L.; Pastor, E. *Langmuir* **2000**, *16*, 4695.
(16) Beltramo, G. L.; Koper, M. T. M. *Langmuir* **2003**, *19*, 8907.
(17) Rosca, V.; Beltramo, G. L.; Koper, M. T. M. *Langmuir* **2005**, *21*, 1448.
(18) Rosca, V.; Koper, M. T. M. *Surf. Sci.* **2005**, *584*, 258.

(19) de Vooys, A. C. A.; Beltramo, G. L.; van Riet, B.; van Veen, J. A. R.; Koper, M. T. M. *Electrochim. Acta* **2004**, *49*, 1307.
(20) de Vooys, A. C. A.; Koper, M. T. M.; van Santen, R. A.; van Veen, J. A. R. *Electrochim. Acta* **2001**, *46*, 923.
(21) Pirug, G.; Bonzel, H. P.; Hopster, H.; Ibach, H. *J. Chem. Phys.* **1979**, *71*, 593.
(22) Gardner, P.; Tueshaus, M.; Martin, R.; Bradshaw, A. M. *Surf. Sci.* **1990**, *240*, 112.
(23) Masel, R. I. *Catal. Rev.-Sci. Eng.* **1986**, *28*, 335.
(24) Tang, C.; Zou, S.; Weaver, M. J. *Surf. Sci.* **1998**, *412*−*413*, 344.
(25) Clavilier, J.; Armand, D.; Sun, S. G.; Petit, M. *J. Electroanal. Chem.* **1986**, *205*, 267.
(26) Feliu, J. M.; Orts, J. M.; Fernandez-Vega, A.; Aldaz, A.; Clavilier, J. *J. Electroanal. Chem.* **1990**, *296*, 191.
(27) Iwasita, T.; Nart, F. C.; Vielstich, W. *Ber. Bunsen-Ges. Phys. Chem.* **1990**, *94*, 1030.
(28) Wonders, A.; Housmans, T. H. M.; Rosca, V.; Koper, M. T. M., submitted.
(29) Clavilier, J.; Feliu, J. M.; Fernandez-Vega, A.; Aldaz, A. *J. Electroanal. Chem.* **1989**, *269*, 175.
(30) Rodes, A.; Clavilier, J.; Orts, J. M.; Feliu, J. M.; Aldaz, A. *J. Electroanal. Chem.* **1992**, *338*, 317.
(31) Al-Akl, A.; Attard, G. A.; Price, R.; Timothy, B. *J. Electroanal. Chem.* **1999**, *467*, 60.
(32) Yeo, Y. Y.; Vattuone, L.; King, D. A. *J. Chem. Phys.* **1996**, *104*, 3810.
(33) Sugai, S.; Takeuchi, K.; Ban, T.; Miki, H.; Kawasaki, K. *Surf. Sci.* **1993**, *282*, 67.
(34) Song, M.-B.; Momoi, K.; Ito, M. *Jpn. J. Appl. Phys.* **1997**, *36*, L1528.
(35) Rienks, E. D. L.; Bakker, J. W.; Baraldi, A.; Carabiniero, S. A. C.; Lizzit, S.; Weststrate, C. J.; Nieuwenhuys, B. E. *Surf. Sci.* **2002**, *516*, 109.
(36) Lesley, M. W.; Schmidt, L. D. *Surf. Sci.* **1985**, *155*, 215.
(37) Kibler, L. A.; Cuesta, A.; Kleinert, M.; Kolb, D. M. *J. Electroanal. Chem.* **2000**, *484*, 73.
(38) Al-Akl, A.; Attard, G. A.; Price, R.; Timothy, B. *Phys. Chem. Chem. Phys.* **2001**, *3*, 3261.
(39) Clavilier, J.; El Achi, K.; Petit, M.; Rodes, A.; Zamakhchari, M. A. *J. Electroanal. Chem.* **1990**, *295*, 333.
(40) Christiansen, P. A.; Hamnett, A. *Techniques and Mechanisms in Electrochemistry*; Blackie Academic and Professional: Glasgow, 1994.
(41) Koper, M. T. M.; Jansen, A. P. J.; Santen van, R. A.; Lukkien, J. J.; Hilbers, P. A. J. *J. Chem. Phys.* **1998**, *109*, 6051.
(42) Ge, Q.; Neurock, M. *J. Am. Chem. Soc.* **2004**, *126*, 1551.
(43) Rosca, V.; Beltramo, G. L.; Koper, M. T. M. *J. Phys. Chem. B* **2004**, *108*, 8294.
(44) Fink, T.; Dath, J. P.; Bassett, M. R.; Imbihl, R.; Ertl, G. *Surf. Sci.* **1991**, *245*, 96.
(45) Bonzel, H. P.; Broden, G.; Pirug, G. *J. Catal.* **1978**, *53*, 96.
(46) Zemlyanov, D. Y.; Smirnov, M. Y.; Gorodetskii, V. V. *React. Kinet. Catal. Lett.* **1994**, *53*, 87.
(47) Zemlyanov, D. Y.; Smirnov, M. Y. *React. Kinet. Catal. Lett.* **1994**, *53*, 97.
(48) Zemlyanov, D. Y.; Smirnov, M. Y.; Gorodetskii, V. V.; Block, J. H. *Surf. Sci.* **1995**, *329*, 61.
(49) Smirnov, M. Y.; Gorodetskii, V. V.; Block, J. H. *J. Mol. Catal. A: Chem.* **1996**, *107*, 359.